Inorganic Chemistry

Article

pubs.acs.org/IC

$Ba_{1.3}Ca_{0.7}SiO_4:Eu^{2+},Mn^{2+}$: A Promising Single-Phase, Color-Tunable Phosphor for Near-Ultraviolet White-Light-Emitting Diodes

Wenzhen Lv,[†,‡] Mengmeng Jiao,[†,‡] Qi Zhao,[†,‡] Baiqi Shao,[†,‡] Wei Lü,[†] and Hongpeng You*[,†]

[†]State Key Laboratory of Rare Earth Resource Utilization, Changchun Institute of Applied Chemistry, Chinese Academy of Sciences, Changchun 130022, P. R. China

[‡]Graduate University of the Chinese Academy of Sciences, Beijing 100049, P. R. China

ABSTRACT: In this paper, Eu^{2+}-doped and Eu^{2+}/Mn^{2+}-codoped $Ba_{1.3}Ca_{0.7}SiO_4$ phosphors were synthesized by means of a conventional solid-state reaction process. The single-phase purity was checked by means of X-ray diffraction and the Rietveld method. Under excitation at 390 nm, the emission spectra of the Eu^{2+}-doped phosphors exhibit a broad-band emission centered at 500 nm caused by the electric dipole allowed transition of the Eu^{2+} ions. The emission spectra of codoped phosphors show one more broad emission centered at 600 nm attributable to the transitions from the $^4T_1(^4G) \rightarrow {}^6A_1(^6S)$ of Mn^{2+} ions. The luminescent color of the codoped phosphors can be easily adjusted from blue to red with variation of the Mn^{2+} content. The energy transfer mechanism from the Eu^{2+} to Mn^{2+} ions in $Ba_{1.3}Ca_{0.7}SiO_4$ phosphors has been confirmed to be the resonant type via dipole−quadrupole interaction, and the critical distance has been calculated quantitatively. All these results demonstrate that the Eu^{2+}/Mn^{2+}-codoped $Ba_{1.3}Ca_{0.7}SiO_4$ phosphors can be a promising single-phase, color-tunable phosphor for near-UV white-light-emitting diodes after a further optimization process. Additionally, a great red shift from 593 to 620 nm has been observed following the increase of Mn^{2+} content, and the phenomenon has been discussed in relation to the changes in the crystal field surrounding the Mn^{2+} ions and the exchange interactions caused by the formation of Mn^{2+} pairs.

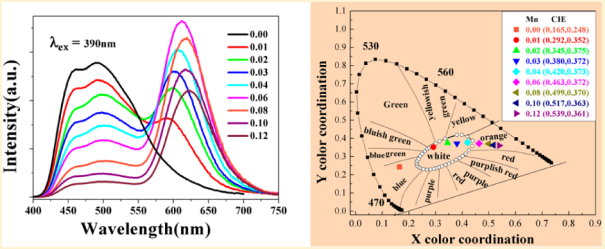

1. INTRODUCTION

Single-phase and color-tunable white light emission phosphors with a near-UV chip have gained more and more attention because of their better color render index and more sufficient color temperature than white-light-emitting diodes (WLEDs) with a multicomponent emitter system for lighting and displays.[1,2] As we know, the strong reabsorption of the blue light often produces the loss of luminous efficiency in phosphor blending systems. However, white light emission in a single phase can avoid this point and enhance the luminescence efficiency. Therefore, the most commonly used way to realize color-tunable white light emission in a single phase is by codoping a sensitizer for the activator, which is based on the theory that nonradiative energy transfer exists between luminescence ions with spectra overlap. The Eu^{2+} ions, a perfect sensitizer, always show broad absorption and emission with higher efficiency since the $4f^7-4f^65d^1$ transition of Eu^{2+} ions is an electric dipole allowed transition and the energy position of the 5d levels is strongly dependent on the host lattice.[3−5] Although, the emission of Mn^{2+} ions is also closely dependent on the crystal field strength, its excitation band is weak, since the absorption and emission are spin-forbidden transitions.[6] Meanwhile, the excitation band is almost not influenced by the host lattice ranging from 400−520 nm with several sharp bands. Consequently, codoping a sensitizer for Mn^{2+} ions is an important method to increase the emission. Due to the adjustability of the 5d level of Eu^{2+} ions, the Eu^{2+} ions can act as a perfect sensitizer for Mn^{2+} ions. As a result, the most important thing is to choose an appropriate host lattice for adjusting the 5d level of Eu^{2+} ions to realize the maximum energy match between Eu^{2+} and Mn^{2+} ions.[7] Now, color tunability in a single phase has been realized in some silicate compounds utilizing the sensitization of Mn^{2+} ions with Eu^{2+} ions. For example, Yang et al. proposed that the Eu^{2+} and Mn^{2+} coactivated $CaAl_2Si_2O_8$ could be a potential phosphor for near-UV WLEDs.[8] This phosphor can also be excited by the near-ultraviolet light and shows various hues by appropriately tuning the activator and sensitizer content. Kim et al. reported that $Sr_3MgSi_2O_8:Eu^{2+},Mn^{2+}$ can be utilized as a phosphor for fabrication of warm WLEDs as well.[9] They have come to the conclusion that the blue (470 nm) band and yellow (570 nm) emission band are originated from the Eu^{2+} ions, while the red (680 nm) emission band is attributed to the Mn^{2+} ions. Very recently, our group has put forward that the $Na_2Ca_4Mg_2Si_4O_{15}:Eu^{2+},Mn^{2+}$ can be an efficient phosphor material for near-UV WLEDs.[10] Eu^{2+} and Mn^{2+} ions codoped silicate phosphors, acting as new single-phase, color-tunable white light emission phosphors for near-UV chips, are attracting widespread attention due to their high efficiency, stable crystal structure, and environmentally friendly characteristics.

Received: June 19, 2014
Published: September 26, 2014

   dx.doi.org/10.1021/ic501423p | *Inorg. Chem.* 2014, 53, 11007−11014

This present work was undertaken to develop a new single-phase, color-tunable Eu^{2+}/Mn^{2+}-doped silicate phosphor. After many failures, we aspire to choose the compound $Ba_{1.3}Ca_{0.7}SiO_4$, whose crystal structure is homeotypic to that of glaserite ($K_3NaS_2O_8$). The Ba, Ca, and Si atoms substitute the sites of K, Na, and S, atoms, respectively.[11,12] The various five Ba/Ca sites in the host make it possible to provide various environments to Eu^{2+} ions for adjusting the 5d energy level to realize various emitting wavelengths. Consequentially, we have synthesized $Ba_{1.3}Ca_{0.7}SiO_4$ samples with various Eu^{2+} or Mn^{2+} concentrations and studied their excitation and emission spectra, decay curves, and thermal stability to clarify their potential to act as an excellent single-phase, color-tunable phosphor for near-UV WLEDs.

2. EXPERIMENTAL SECTION

2.1. Preparation. Polycrystalline phosphor samples with the compositions of $Ba_{1.3-x}Ca_{0.7-y}SiO_4:xEu^{2+},yMn^{2+}$ (BCSO:xEu^{2+},yMn^{2+}) were prepared by the high temperature solid state reaction process. The stoichiometric amounts of [$CaCO_3$ (AC), $BaCO_3$ (AC), SiO_2 (AC), Eu_2O_3 (99.99%), and $MnCO_3$ (99.99%)] were weighed out and ground in an agate mortar to mix them homogeneously. Afterward, the powder mixtures were fired in a reducing atmosphere N_2/H_2 at 1100−1200 °C for 3−4 h to obtain the final products.

2.2. Characterization. The X-ray diffraction (XRD) data of all the samples were collected using a D8 Focus diffractometer (Bruker) operating at 40 kV and 40 mA with Cu Kα radiation. The scanning rate was fixed at 0.5°/min and 0.02°/step with 2θ ranging from 10° to 90°. Crystal structure refinement employed the Rietveled method as implemented in the General Structure Analysis System software suite.[13] The excitation and emission spectra were measured with a Hitachi F-4500 spectrophotometer equipped with a 150 W xenon lamp as the excitation source. Absolute photoluminescence quantum yields data were collected by an absolute PL quantum yield measurement system (C9920-02, Hamamatsu Photonics K. K.). As to the luminescence decay curve, all of the results were obtained from a Lecroy Wave Runner 6100 digital oscilloscope (1 GHz) using a tunable laser (pulse width = 4 ns, gate = 50 ns) as the excitation source (Continuum Sunlite OPO). The temperature-dependent properties of the phosphors were measured on an Edinburgh Instrument FLS 920 spectrophotometer with an Advanced Research System Inc. temperature controlling system.

3. RESULTS AND DISCUSSION

3.1. Phase Identification. Some representative XRD patterns of BCSO:xEu^{2+},yMn^{2+} samples are illustrated in Figure 1. All the observed peaks matches well with JCPDS file no. 48-0210, indicating a single phase formed without detectable impurities.[11] Figure 2a shows the Rietveld refinement result of BCSO:0.01Eu^{2+} phosphor, including the experimental patterns, calculated patterns, the differences between the experimental and calculated patterns, and the Bragg reflections of the calculated patterns. The detailed final structural parameters have been summarized in Table 1. The obtained fitted parameters are χ^2 = 8.319, R_P = 8.28%, and R_{WP} = 5.92%. According to the refinement results, it can be known that the crystal structure of $Ba_{1.3}Ca_{0.7}SiO_4$ is built of five kinds of Ba/Ca sites (one 6-fold coordination, two 10-fold coordination, and two 12-fold coordination) and anion group SiO_4^{4-} tetrahedra. Figure 2b shows a unit cell of $Ba_{1.3}Ca_{0.7}SiO_4$ and the coordination environment of the five Ba/Ca sites. The Ba/Ca sites with same coordination have similar Ba/Ca−O crystal coordination environment.

The radius percentage discrepancy (Dr) between the doped ions and the possible occupied ions (Ca^{2+}, Ba^{2+}) in

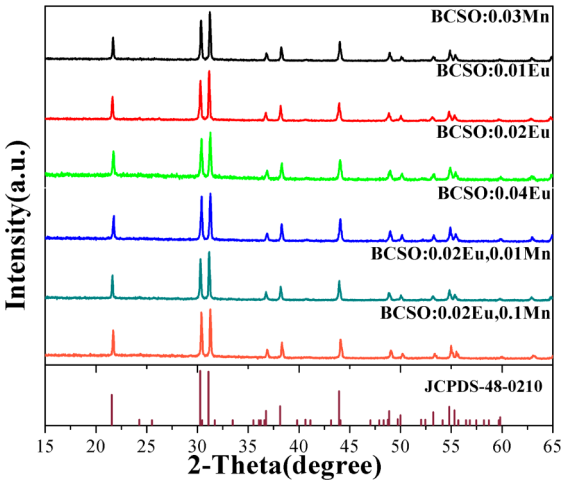

Figure 1. Powder X-ray diffraction patterns for several representative BCSO:xEu^{2+},yMn^{2+} samples.

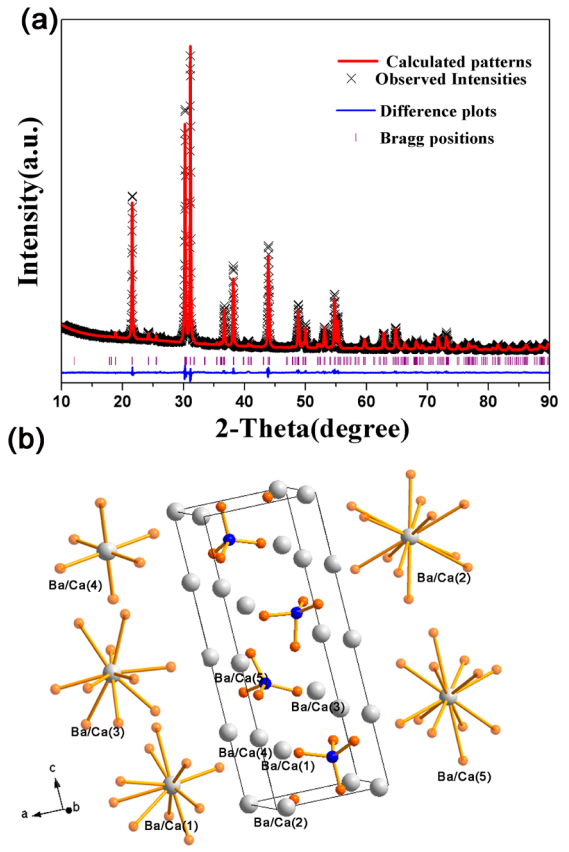

Figure 2. (a) Rietveld refinement of the XRD profile of BCSO:0.01Eu^{2+}. (b) Structural view of a unit cell of $Ba_{1.3}Ca_{0.7}SiO_4$ and coordination environments for Ba/Ca sites.

$Ba_{1.3}Ca_{0.7}SiO_4$ have been calculated for the purpose of investigating the occupied situation of the doped ions (Eu^{2+}, Mn^{2+}). The calculation is based on the following formula[14]

$$\mathrm{Dr} = 100 \times \frac{R_m(\mathrm{CN}) - R_d(\mathrm{CN})}{R_m(\mathrm{CN})} \quad (1)$$

where CN is the coordination number, R_m(CN) is the radius of the host cations, and R_d(CN) is the radius of doped ion. We cannot do the corresponding calculation for Mn^{2+} with CN =

dx.doi.org/10.1021/ic501423p | Inorg. Chem. 2014, 53, 11007−11014

Table 1. Refinement and Crystallographic Data of $Ba_{1.3}Ca_{0.7}SiO_4$:0.01Eu^{2+}

formula	$Ba_{1.3}Ca_{0.7}SiO_4$:0.01Eu^{2+}
X-ray source	Cu Kα
T/K	297
symmetry	hexagonal
space group	$P\bar{3}m1$
a/Å	5.758
b/Å	5.758
c/Å	14.714
volume/Å^3	422.54
Z	2
R_P/%	8.28
R_{WP}/%	5.92
χ^2	8.319

10 and 12 owing to lack the reference data. Table 2 has shown the Dr between matrix cations and doped ions. From the Dr of

Table 2. Ionic Radii Discrepancy Percentage (Dr) between the Doped Ions and Matrix Cations

		Dr/%	
		Ca(6) 1.00 Å	Ba(6) 1.35 Å
		Ca(10) 1.23 Å	Ba(10) 1.52 Å
doped ion	radius/Å (CN[a])	Ca(12) 1.34 Å	Ba(12) 1.61 Å
Eu^{2+}	1.17 (6)	−17	13
	1.35 (10)	−9.7	11.2
	1.48 (12)	−10.4	8.1
Mn^{2+}	0.83 (6)	17	38.5

[a]CN = coordination number.

Eu^{2+} substituted for $Ca^{2+}$and Ba^{2+}, we can get the conclusion that the Eu^{2+} ions prefers to substitute the site of Ba^{2+}. While Dr of Mn^{2+} for Ca^{2+} is smaller than that for Ba^{2+}. As a result, the doped ion Mn^{2+} will substitute the Ca site clearly. Therefore, combining the Dr and valence state of Eu^{2+}/Ba^{2+} and Mn^{2+}/Ca^{2+} ions, we suppose that the Eu^{2+} and Mn^{2+} prefer to substitute the Ba^{2+} and Ca^{2+} sites, respectively.

3.2. Luminescence Properties of BCSO:Eu^{2+} Phosphors. Figure 3 presents the excitation and emission spectra of BCSO:0.04Eu^{2+} sample. With the near-UV excitation at 400 nm, the emission spectrum shows a very strong broad blue

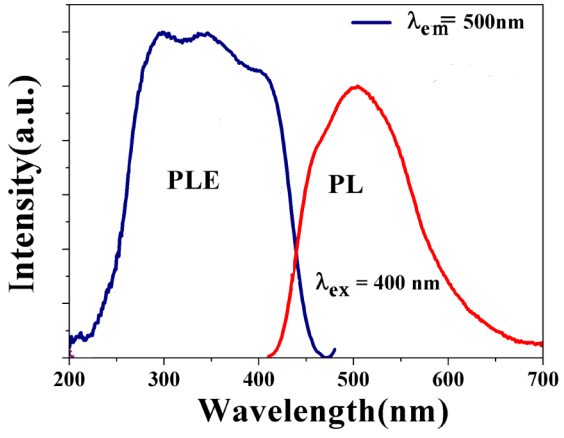

Figure 3. Emission and excitation spectra of BCSO:0.04Eu^{2+} phosphor.

green emission band peaking at 500 nm. Monitored at 500 nm, one can see clearly that the excitation spectrum is formed by a broad band extending from 200 to 450 nm. This broad band can be ascribed to the characteristic excitation resulting from the parity-allowed $4f^7(^8S_{7/2}) \rightarrow 4f^65d^1$ transitions of the Eu^{2+} ion.[15,16] Also, it seemed that the emission spectrum is asymmetric on the long wavelength side, which may result from the various Eu^{2+} ions sites in the lattice. For the purpose of understanding thoroughly this phenomenon, a series of samples as a function of Eu^{2+} content have been worked out, and the corresponding normalized emission spectra and the emission intensity variations are shown in Figure 4. From the

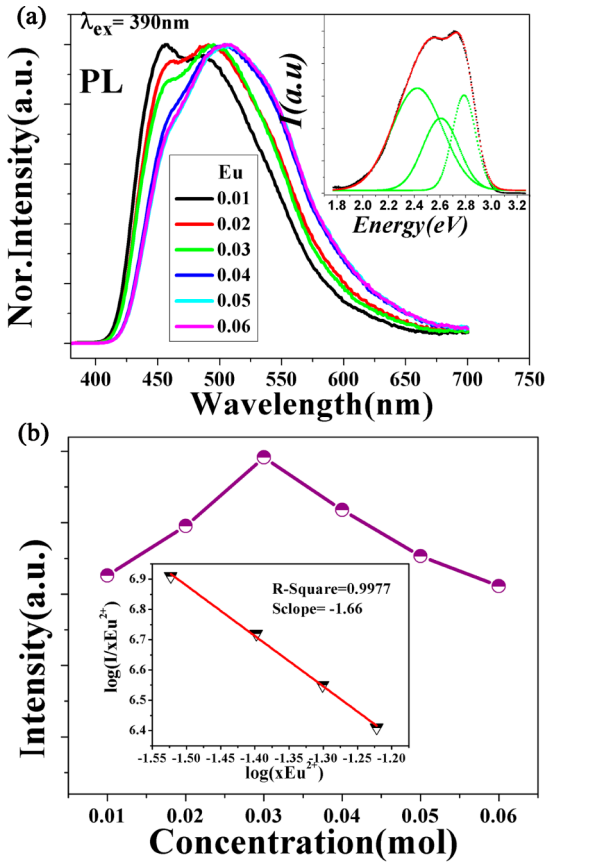

Figure 4. (a) Normalized emission intensity of BCSO:$x$$Eu^{2+}$ with various Eu^{2+} concentrations. The inset shows the BCSO:0.01Eu^{2+} phosphor fitted with a total of three Gaussian functions on energy level. (b) Emission intensity of BCSO:$x$$Eu^{2+}$ with various Eu^{2+} concentration (λ_{ex} = 390 nm). The inset presents the plot log(I/$x$$Eu^{2+}$) versus log($x$$Eu^{2+}$).

normalized emission spectra at low concentration, a peak at about 460 nm can be seen clearly; however, it disappears with an increase of content of Eu^{2+} ions. Also, a continuous red shift can be observed clearly until x = 0.04. To the best of our knowledge, the variations of the normalized emission spectra may indicate that the occupation of the Eu^{2+} ions changes with its increasing doped content. We fit the emission spectrum with the Gaussian function of BCSO:0.01Eu^{2+} phosphor on its energy level, which is been shown in the inset of Figure 4a. The green dotted line denotes three Gaussian functions successfully fit with maxima at 446 nm (2.78 eV), 475 nm (2.61 eV), and 512 nm (2.42 eV), respectively. These different emission wavelengths are caused by the different crystal surroundings of

dx.doi.org/10.1021/ic501423p | Inorg. Chem. 2014, 53, 11007−11014

the various Eu^{2+} ions sites, so it can be presumed that there are three various emission centers in this host. According to crystal field theory, luminescence centers with similar coordinate environment are spectrally undistinguishable. From the former structural analysis, both the crystallographic sites of the two (Ba/Ca) O_{10} and the two (Ba/Ca) O_{12} have similar surroundings, respectively. The Eu^{2+} ions at these sites are too close to be clearly distinguished, so the two (Ba/Ca) O_{10} and two (Ba/Ca) O_{12} can be understood as two independent luminescence centers. As a result, the three Gaussian peaks are in agreement with the three independent luminescence centers. The emission intensity begins to enhance with the increase of Eu^{2+} concentration and achieves the maximum value at x = 0.03, and then it decreases at higher concentrations, which can be attributable to the nonradiative transition of the increasing Eu^{2+} ions. The interatomic distance of Eu^{2+} ions is compressed with the increase of concentration and it makes the nonradiative transition of Eu^{2+} ions gain a higher relaxation rate from excited to ground state. Another explanation for this phenomenon is the concentration quenching of inorganic materials.[17]

On the basis of the Dexter's theory, the emission intensity (I) per activator ion can be presented by the following formula[18]

$$\frac{I}{x} = K[1 + \beta(x)^{Q/3}]^{-1} \quad (2)$$

where Q = 6, 8, 10 is corresponding to dipole−dipole (d−d), dipole−quadrupole (d−q), and quadrupole−quadrupole (q−q) interaction, respectively. x is the activator concentration, and K and β are unchanging for the same excitation circumstance for a certain host. The inset of Figure 4b presents a plot of $\log(x\mathrm{Eu}^{2+})$ vs $\log(I/x\mathrm{Eu}^{2+})$, and the fitted result is liner and the scope is −1.66. According to the above equation, the Q value is estimated to be 4.98. This value means that the concentration quenching mechanism here is based on a d−d interaction.

3.3. Luminescence Properties of BCSO:Mn^{2+} and BCSO:Eu^{2+},Mn^{2+} Phosphors. Figure 5 displays the excitation and emission spectra of BCSO:0.09Mn^{2+} phosphor. According to Tanabe−Sugano diagrams of Mn^{2+} ions, these sharp lines ranging from 400 to 520 nm in the excitation spectrum can be associated with the well-known transitions from the ground state $^6A_1$ to the excited states $^4E(^4D)$, $^4T_2(^4D)$, $[^4A_1(^4G), ^4E(^4G)]$, $^4T_2(^4G)$, and $^4T_1(^4G)$.[19] However, these absorptions are very weak because of the spin-forbidden characteristic of Mn^{2+} ions. The emission spectrum is composed of a wide symmetric band peaking at 610 nm attributed to the spin-forbidden d−d transition $[^4T_1(^4G) \rightarrow {}^6A_1(^6S)]$ of the Mn^{2+} ions. The wide emission of Mn^{2+} ions that ranges from 500 to 700 nm is strongly related to the ligand field strength and coordination number. The stronger ligand field strength always produces the longer the emission position. The coordination number also has an enormous influence on the emission wavelength. Usually, the Mn^{2+} ions can give various emissions (green to red) with increasing coordination number. Here, the phosphor emits a wide red emission band centered at about 610 nm. Combining former structure analysis, we consider that the Mn^{2+} ions prefer to substitute the Ca^{2+} site with hexahedral coordination.[20]

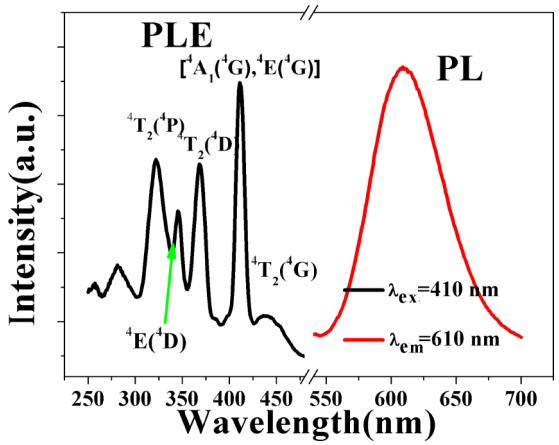

Figure 5. Excitation and emission spectra of BCSO:0.09Mn^{2+} phosphor.

A usually necessary condition for energy transfer is the spectra overlap between the donor emission band and the acceptor excitation band. According to above analysis, the emission spectrum of the Eu^{2+} ions apparently overlaps the excitation spectrum of the Mn^{2+} ions, which makes it possible to realize the energy transfer from Eu^{2+} ions to Mn^{2+} ions. The excitation and emission spectra of BCSO:0.02Eu^{2+},0.04Mn^{2+} phosphor are shown in Figure 6. The excitation spectrum

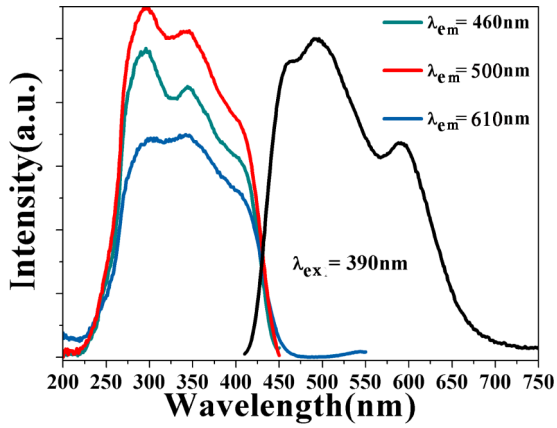

Figure 6. Excitation and emission spectra of BCSO:0.02Eu^{2+},0.04Mn^{2+} phosphor.

monitored by the emission of Mn^{2+} ions is in accord with that of the Eu^{2+} ions, revealing the performance of energy transfer from the Eu^{2+} to Mn^{2+} ions. Under the excitation at 390 nm, the emission spectrum of BCSO:0.02Eu^{2+},0.04Mn^{2+} displays a red emission band ascribed to the Mn^{2+} ions in addition to a broad blue green emission band corresponding to the Eu^{2+} ions. Hence, a color-tunable emission can be achieved by adjusting the emission of the Eu^{2+} and Mn^{2+} ions in the lattice.

To obtain some information about the relation between the tunable emission and the Mn^{2+} contents, we have prepared a series of samples as a function of Mn^{2+} ion content. Figure 7 presents the emission spectra of BCSO:0.02Eu^{2+},$y$$Mn^{2+}$ (y = 0.01, 0.02, 0.03, 0.04, 0.06, 0.08, 0.10, 0.12) phosphors under the excitation of 390 nm. The emission intensity of Eu^{2+} is found to decline monotonically with an increase of Mn^{2+} ion content. However, the emission intensity of Mn^{2+} ions achieves the maximum value at y = 0.06 and then begins to drop, which is ascribed to energy reabsorption among the nearest Eu^{2+} or Mn^{2+} ions. Additionally, an obvious red shift can be found with the increase of Mn^{2+} concentration. The peak of the emission increases from 593 to 620 nm with the y from 0.01 to 0.12 mol,

dx.doi.org/10.1021/ic501423p | Inorg. Chem. 2014, 53, 11007−11014

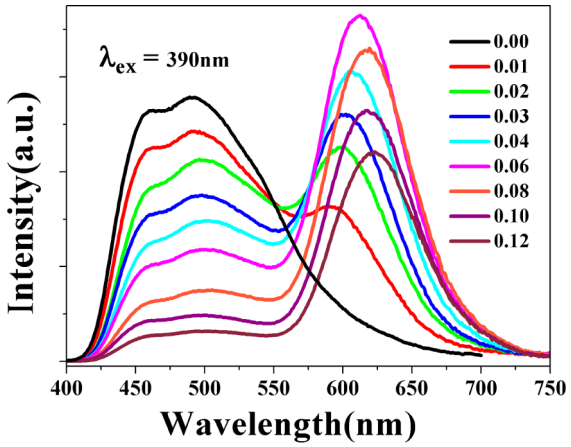

Figure 7. Emission spectra of BCSO:0.02Eu^{2+},yMn^{2+} (y = 0.01, 0.02, 0.03, 0.04, 0.06, 0.08, 0.10, 0.12) phosphors under 390 nm excitation.

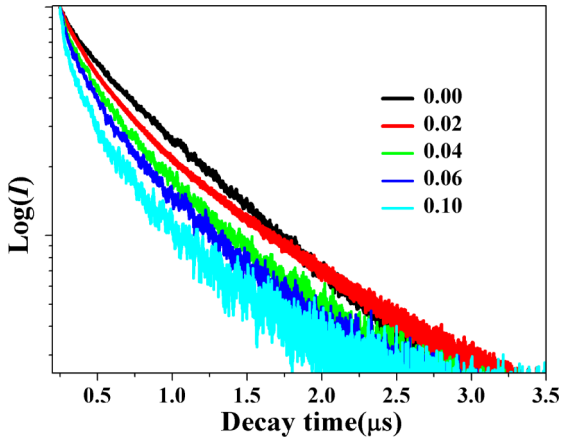

Figure 8. Luminescence decay curves of Eu^{2+} ions in BCSO:0.02Eu^{2+},yMn^{2+} (y = 0.00, 0.02, 0.04, 0.06, 0.10) phosphors (monitored at 490 nm, excited at 355 nm).

and it can be explained by the changing crystal field surroundings around Mn^{2+} ions. A measure of the crystal field strength (D_q) around Mn^{2+} ions can be depicted as follows[21]

$$D_q = \frac{ze^2r^4}{6R^5} \quad (3)$$

where R is the bond length, z is the anion charge, e is the electron charge, and r is the d wave function radius. As a result, the bonds length of the luminescent ions is closely related to the emission wavelength for a given luminescent ion. On the basis of the former analysis, we know that the Mn^{2+} ions prefer to substitute for the larger Ca^{2+} ions, which could lead to a shortening of the bond length and result in the enhancement of crystal field strength. As a result, the stronger crystal field strength makes the lowest d state of Mn^{2+} ions closer to the ground state and finally produces the red shift. Another explanation of the red shift is the exchange interaction between Mn^{2+} ion pairs. In heavily Mn^{2+}-doped samples, due to the formation of Mn^{2+} pairs, their interaction by exchange interaction reduces the energy discrepancy between the ground and first excited states, which would yield red shift emission as well.[22]

When the sensitizer ions with a random distribution are excited, each ion has the same probability for a radiative decay, resulting in purely exponential fluorescence decay. However, when the activator ions are also present and randomly distributed in the medium, some of the excited sensitizer ions will transfer energy to the sufficiently close activator ions. In another words, the codoped phosphors often provide more channels for the intensity decline of sensitizer, accelerating the decay process. Generally, the lifetime is always defined as the value when the instantaneous intensity decreases to $^1/_e$ of the initial intensity. So another direct evidence to verify the energy transfer process is to compare the lifetime value of Eu^{2+} ions in the single doped and codoped samples.[23] Figure 8 presents the decay curves of some samples. Here, the decay path of Eu^{2+} ions is complicated due to the diverse cation sites in the host lattice, so the lifetime value was given as the effective lifetime defined as follows[24]

$$\tau^* = \frac{\int_0^\infty tI(t)\,dt}{\int_0^\infty I(t)\,dt} \quad (4)$$

The calculated average lifetime of Eu^{2+} ions of BCSO:0.02Eu^{2+},yMn^{2+} (y = 0.00, 0.02, 0.04, 0.06, and 0.10) samples is 0.605, 0.509, 0.439, 0.389, and 0.305 μs. The lifetime value decreases monotonically with the increasing Eu^{2+} ions. This is a powerful proof for the energy transfer from Eu^{2+} to Mn^{2+} ions.

According to the theory of Paulose et al., the energy transfer efficiency (η) from the Eu^{2+} to Mn^{2+} ions can be presented as the following equation[25]

$$\eta = 1 - \frac{I_S}{I_{S0}} \quad (5)$$

where I_{S0} and I_S are the emission intensities of the Eu^{2+} ions in the absence and presence of Mn^{2+}. The energy transfer efficiency has been calculated to be 16.6%, 26.8%, 39.5%, 48.6%, 59.3%, 74.0%, 83.1%, and 88.7%, corresponding to y = 0.01, 0.02, 0.03, 0.04, 0.05, 0.06, 0.08, 0.10, and 0.12. This result indicates that the energy transfer efficiency value enhances monotonically with the increase of Mn^{2+} content.

Table 3 summarizes the CIE chromaticity coordinates of BCSO:0.02Eu^{2+},yMn^{2+} (0, 0.01, 0.02, 0.03, 0.04, 0.06, 0.08, 0.10, 0.12) samples excited at 390 nm. All the values are calculated on the basis of the corresponding emission spectrum, which are also depicted as Figure 9. The chromaticity coordinates (X, Y) for BCSO:0.02Eu^{2+},yMn^{2+} phosphors were measured as (0.165, 0.248), (0.292, 0.352), (0.345, 0.375), (0.380, 0.372), (0.420, 0.378), (0.463, 0.372), (0.499, 0.370),

Table 3. Comparison of the CIE Coordinates (X, Y), CCT, and Quantum Efficiency (QY) for BCSO:0.02Eu^{2+},yMn^{2+} under 390 nm Excitation

sample	Mn^{2+} content (y)	CIE coordinates (X, Y)	CCT/K	QY/%
1	0.00	(0.165, 0.248)	98976	53
2	0.01	(0.292, 0.352)	7412	48
3	0.02	(0.345, 0.375)	5076	43
4	0.03	(0.380, 0.372)	3952	38
5	0.04	(0.420, 0.378)	2956	32
6	0.06	(0.463, 0.372)	2199	28
7	0.08	(0.499, 0.370)	1879	20
8	0.10	(0.517, 0.363)	1880	11
9	0.12	(0.539, 0.361)	2091	8

dx.doi.org/10.1021/ic501423p | Inorg. Chem. 2014, 53, 11007−11014

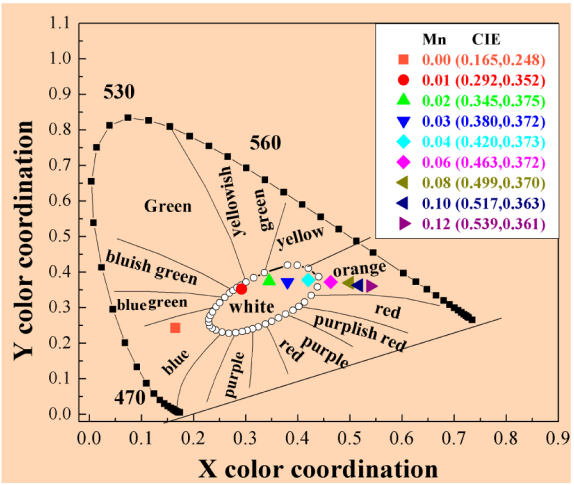

Figure 9. CIE chromaticity diagram of BCSO:0.02Eu^{2+},yMn^{2+} (y = 0, 0.01, 0.02, 0.03, 0.04, 0.06, 0.08, 0.10, 0.12) phosphors under 390 nm excitation.

(0.517, 0.363), and eventually (0.539, 0.361) with x = 0, 0.01, 0.02, 0.03, 0.04, 0.06, 0.08, 0.10, 0.12, respectively. The connecting line of all color points runs though the white region. As a result, the color of the phosphor is tunable from blue to white and finally to orange by systematically adjusting the Mn^{2+} concentration. So this material has a lot of capacity to act as a single phase phosphor for ultraviolet WLEDs. As we know, incident fluxes always quench the phosphor via saturation, which resulted from the high light flux incident on the phosphors in the lamp and the slow radiative relaxation rate of Mn^{2+}. Especially, this situation can be decreased by utilizing a lamp designed to reduce the incident flux on Eu^{2+}/Mn^{2+}-codoped phosphors.[26] The correlated color temperature (CCT) of all the samples is shown in Table 3. The white light emission with different CCT can be realized to meet the need for practical application in near-UV WLEDs by simply adjusting the Mn^{2+} content. As to the abnormal CCT values for the codoped content of Mn^{2+} about 0.12, they may be caused by the concentration quenching. The concentration quenching often makes the energy distribution of the emission spectra different from each other for the samples. As we know, white light emission in the single phase is theoretical, as there is no such compound used in industry, so there is no clear standard to assess the good or bad phosphors, especially under these experimental conditions. In a practical sense, quantum yields are an important parameter for assessing the performance of phosphors. Table 3 also gives the absolute quantum yield (QY) values of BCSO:0.02Eu^{2+},yMn^{2+} (y = 0, 0.01, 0.02, 0.03, 0.04, 0.06, 0.08, 0.10, 0.12) samples excited at 390 nm. The BCSO:0.02Eu^{2+} has the highest QY value of 53% and the other codoped samples show a consequent decline with increasing Mn^{2+} concentration, which is unsatisfying. However, optimizing the sample synthesis process could lead to improvement in the overall phosphor efficiency.

The resonant energy transfer mechanism from sensitizer to activator in lattice is mainly composed of exchange interaction and multipolar interaction according to Dexter theory. Here, the critical distance (R_C) for the energy transfer can be calculated by utilizing the concentration quenching. As a result, the R_C can be calculated as[27]

$$R_C = 2\left[\frac{3V}{4\pi x_c N}\right]^{1/3} \quad (6)$$

where N is the number of sites that the Eu^{2+} can substitute per unit cell, x_c is the critical concentration, and V is the volume of a unit cell. In our case, N = 2, V is estimated to be 420.14 $Å^3$. With the hypothesis that the lattice parameters are unchanged and the critical concentration is about 0.07 from the overall concentration of the Eu^{2+} and Mn^{2+} ions, where η is 0.5, the R_C obtained is about 17.8 Å on the basis of the above equation. To our best knowledge, the critical distance between the sensitizer and activator is always shorter than 3−4 Å for the exchange interaction case. So the quenching mechanism of the Eu^{2+} ions here is mainly decided by the multipolar interaction case.

On the basis of the energy transfer expression of multipolar interaction deduced by Dexter and by Reisfeld's approximation, the next relationship can be given as[28]

$$\frac{I_{S0}}{I_S} \propto C^{n/3} \quad (7)$$

where I_{S0} and I_S are the emission intensities of sensitizer with and without the activator. C is the total of doping concentration of the Eu^{2+} and Mn^{2+} ions, and n = 6, 8, and 10 corresponds to d−d, d−q, and q−q interactions. Figure 10 presents the plots of I_{S0}/I_S versus $C^{n/3}$. It should be noted that for a linear relation only n = 8 provides the best fit and the others fits are slightly beyond the experimental result. The result reveals that the energy transfer mechanism from Eu^{2+} to Mn^{2+} is the d−q interaction.

A thorough knowledge of the thermal quenching of phosphors has a great significance on their further application in industry. Thermal quenching always occurs due to the nonradiative transition from the excited state of luminescent ions to the bottom of conduction band in the lattice. Always, the configurational coordinate diagram can be used to explain thermal quenching. The excited luminescence center is thermally activated through the level crossing point between the excited state and the ground state in that diagram. As a result, the luminescence intensity dependence on the temperature can be depicted by the Arrhenius formula[29,30]

$$I_T = \frac{I_0}{1 + c\,\exp\left(-\frac{\Delta E}{kT}\right)} \quad (8)$$

where I_T corresponds to the intensity of a given temperature, I_0 is the initial intensity, k is Boltzmann's constant (8.619×10^{-5} eV K^{-1}), c is a constant for a given host, and ΔE is the activation energy in relation with the process from the relaxed excited level to the ground level, and the value of ΔE can be a measurement of the thermal stability of the host lattice. For comparison, Figure 11 plots the $\ln(I_0/I_T - 1)$ against $1/kT$ of BCSO:0.02Eu^{2+} and BCSO:0.02Eu^{2+},0.01Mn^{2+} in air from 293 to 473 K. The ΔE was obtained to be about 0.2833 and 0.2479 eV, respectively. The lower activation energy would cause a greater probability for a nonradiative transition. As a result, the BCSO:0.02Eu^{2+} phosphor offers better thermal stability compared with the BCSO:0.02Eu^{2+},0.01Mn^{2+} phosphor. Following the increasing Mn^{2+} ions concentration in host, the number of defects of the host lattice caused by radius differences may increase greatly, which would have considerable influence on the lattice structure. These defects, acting as the nonradiative recombination centers, are responsible for the

dx.doi.org/10.1021/ic501423p | Inorg. Chem. 2014, 53, 11007−11014

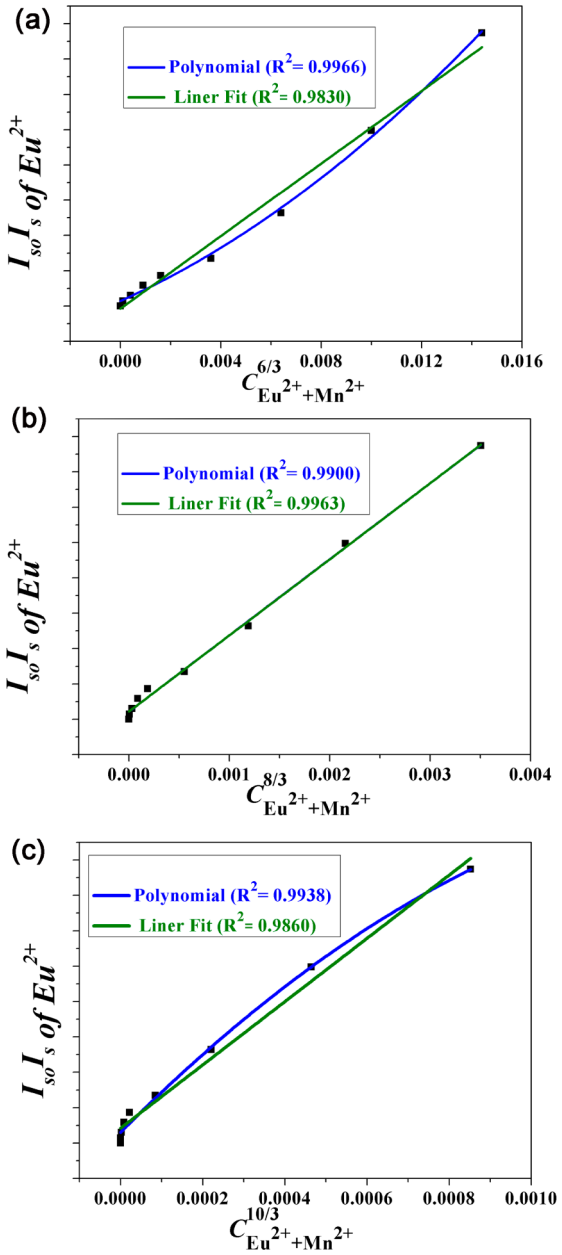

Figure 10. Dependence of I_{S0}/I_S on $Eu^{2+}$and Mn^{2+} ions concentration: (a) $C^{6/3}$, (b) $C^{8/3}$, and (c) $C^{10/3}$.

rapid thermal quenching of Eu^{2+} luminescence. Besides, the reaction process, the raw materials, the best doped content, and other factors all need further optimization to achieve the best performance of this new phosphor to obtain a better thermal stability.

4. CONCLUSION

To sum up, we have prepared new Eu^{2+}-doped and Eu^{2+}/Mn^{2+}-codoped $Ba_{1.3}Ca_{0.7}SiO_4$ silicate phosphors. Luminescence properties reveal that the luminescent color of the phosphor is tunable from blue to white by adjusting the Mn^{2+} concentration. The energy transfer mechanism from the Eu^{2+} to Mn^{2+} ions has been certified to be a dipole−quadrupole interaction, and the critical distance was estimated to be 17.8 Å by utilizing a concentration quenching method. A red shift in the codoped samples has been explained by the changes in the

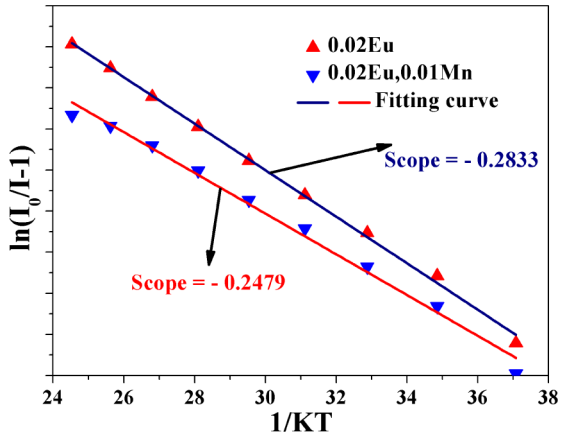

Figure 11. Activation energy (ΔE) of BCSO:0.02Eu^{2+} and BCSO:0.02Eu^{2+},0.01Mn^{2+} phosphors under 365 nm excitation.

crystal field and the exchange interaction caused by the formation of the Mn^{2+} ions pairs. The thermal stability diversities of the single doped and codoped samples are attributed to the defects caused by the increasing doped luminescent ions. Therefore, preliminary studies demonstrate that the obtained phosphor shows tremendous potential in near-UV WLEDs.

AUTHOR INFORMATION

Corresponding Author

*Fax: +86-431-85698041. Tel: +86-431-85262798. E-mail: hpyou@ciac.ac.cn.

Notes

The authors declare no competing financial interest.

ACKNOWLEDGMENTS

This work is financially supported by the National Natural Science Foundation of China (Grant No. 21271167), the Fund for Creative Research Groups (Grant No. 21221061), and the National Basic Research Program of China (973 Program, Grant No. 2014CB6438003).

REFERENCES

(1) Feldmann, C.; Justel, T.; Ronda, C. R.; Schmidt, P. J. *Adv. Funct. Mater.* **2003**, *12*, 511−516.
(2) Lin, C. C.; Liu, R. S. *J. Phys. Chem. Lett.* **2011**, *2*, 1268−1277.
(3) Li, X.; Budai, J. D.; Liu, F.; Howe, J. Y.; Zhang, J.; Wang, X.; Gu, Z.; Sun, C.; Meltzer, R. S.; Pan, Z. *Light Sci. Appl.* **2013**, *2*, e50.
(4) Liu, C.; Qi, Z.; Ma, C.; Dorenbos, P.; Hou, D.; Zhang, S.; Kuang, X.; Zhang, J.; Liang, H. *Chem. Mater.* **2014**, *26*, 3709−3715.
(5) Denault, K. A.; Brgoch, J.; Gaultois, M. W.; Mikhailovsky, A.; Petry, R.; Winkler, H.; DenBaars, S. P.; Seshadri, R. *Chem. Mater.* **2014**, *26*, 2275−2282.
(6) Chan, T. S.; Liu, R. S.; Baginskiy, I. *Chem. Mater.* **2008**, *20*, 1215−1217.
(7) Guo, C.; Luan, L.; Ding, X.; Huang, D. *Appl. Phys. A: Mater. Sci. Process.* **2008**, *91*, 327−331.
(8) Yang, W. J.; Luo, L.; Chen, T. M.; Wang, N. S. *Chem. Mater.* **2005**, *17*, 3883−3888.
(9) Kim, J. S.; Jeon, P. E.; Park, Y. H.; Choi, J. C.; Park, H. L.; Kim, G. C.; Kim, T. W. *Appl. Phys. Lett.* **2004**, *85*, 3696.
(10) Lv, W.; Jia, Y.; Zhao, Q.; Jiao, M.; Shao, B.; Lü, W.; You, H. *RSC Adv.* **2014**, *4*, 7588−7593.
(11) Fukuda, K.; Ito, M.; Iwata, T. *J. Solid State Chem.* **2007**, *180*, 2305−2309.

(12) Fang, Y.; Li, L.; Chen, Y.; Wang, H.; Zeng, R. *J. Lumin.* **2013**, *144*, 13−17.
(13) Larson, A. C.; Von Dreele, R. B. *General Structure Analysis System (GSAS)*; Los Alamos National Laboratory Report LAUR 86-748, 2004.
(14) Peng, M.; Pei, Z.; Hong, G.; Su, Q. *J. Mater. Chem.* **2003**, *13*, 1202−1205.
(15) Lucas, F.; Jaulmes, S.; Quarton, M.; Le Mercier, T.; Guillen, F.; Fouassier, C. *J. Solid State Chem.* **2000**, *150*, 404−409.
(16) Blasse, G. *Phys. Status Solidi B* **1973**, *55*, K131−K134.
(17) Zhang, X.; Tang, X.; Zhang, J.; Gong, M. *J. Lumin.* **2010**, *130*, 2288−2292.
(18) Van Uitert, I. G. *J. Electrochem. Soc.* **1967**, *114*, 1048−1053.
(19) Zhang, S.; Liang, H.; Liu, Y.; Liu, Y.; Hou, D.; Zhang, G.; Shi, J. *Opt. Lett.* **2012**, *37*, 2511−2513.
(20) Shi, L.; Huang, Y.; Seo, H. J. *J. Phys. Chem. A* **2010**, *114*, 6927−6934.
(21) Rack, P. D.; Holloway, P. H. *Mater. Sci. Eng.* **1998**, *21*, 171−219.
(22) Lü, J.; Du, F.; Zhu, R.; Huang, Y.; Seo, H. J. *J. Mater. Chem.* **2011**, *21*, 16398−16405.
(23) Han, J. Y.; Im, W. B.; Lee, G.; Jeon, D. Y. *J. Mater. Chem.* **2012**, *22*, 8793−8798.
(24) Guo, N.; You, H.; Jia, C.; Ouyang, R.; Wu, D. *Dalton Trans.* **2014**, *43*, 12373−12379.
(25) Paulose, P. I.; Jose, G.; Thomas, V.; Unnikrishnan, N. V.; Warrier, M. K. R. *J. Phys. Chem. Solids* **2003**, *64*, 841−846.
(26) Setlur, A. A.; Shiang, J. J.; Happek, U. *Appl. Phys. Lett.* **2008**, *92*, 081104.
(27) You, H.; Zhang, J.; Hong, G.; Zhang, H. *J. Phys. Chem. C* **2007**, *111*, 10657−10661.
(28) Kwon, K. H.; Im, W. B.; Jang, H. S.; Yoo, H. S.; Jeon, D. Y. *Inorg. Chem.* **2009**, *48*, 11525−11532.
(29) Lv, W.; Jia, Y.; Zhao, Q.; Jiao, M.; Shao, B.; Lü, W.; You, H. *Adv. Opt. Mater.* **2014**, *2*, 183−188.
(30) Xie, R.; Hirosaki, N.; Kimura, N.; Sakuma, K.; Mitomo, M. *Appl. Phys. Lett.* **2007**, *90*, 191101.